Kovine, zlitine, tehnologije / letnik 27 / številka 1–2 / strani 9 do 20 / 1993

Surface and Grain Boundary Segregation on and in Iron and Steels — Effects on Steel properties

Segregacije na površini in na mejah zrn železa in jekla — vplivi na lastnosti jekel

H.J. Grabke, *Max-Planck-Institut für Eisenforschung GmbH, Düsseldorf, Deutschland*

The surface and grain boundary segregation was studied for binary alloys Fe-A using Auger-Electron Spectroscopy, Low Energy Electron Diffraction and Photoelectron-Spectroscopy. As examples the surface segregation of C, Si, Sn, O, and S on iron and the grain boundary segregation of P and Sn are described. The segregation studies are correlated to metallurgical phenomena: the effect of sulfur on carburization and nitrogenation, the effects of phosphorus at grain boundaries on embrittlement of a turbine steel and stress corrosion cracking of carbon steels and the effect of tin on the creep of a turbine steel.

Key words: surface segregation, grain boundary segregation, segregation thermodynamics, segregation structures, surface reactions, surface diffusion, intergranular fracture, embrittlement of steels, intergranular corrosion, Langmiur-McLean creep of heat resistant steels

Segregacije na površini in na mejah zrn binarnih zlitin Fe-A so bile raziskane z metodami AES (spektroskopija Augerjevih elektronov), LEED (nizkoenergijski elektronski uklon) in XPS (rentgenska fotoelektronska spektroskopija). Opisani so primeri segregacij C, Si, Sn, O in S na površini železa in P ter Sn na mejah zrn. Raziskave segregacij so povezane z metalurškimi procesi in pojavi: vpliv žvepla na naogljičenje in nitriranje, vpliv fosforja na mejah zrn na krhkost jekel za turbine in na napetostne korozijske razpoke ogljikovih jekel ter vpliv kositra na lezenje jekel za turbine.

Ključne besede: segregacije na površini, segregacije na mejah zrn, termodinamika segregacije, struktura segregacije, reakcije na površini, difuzija na površini, interkristalni prelom, krhkost jekel, lezenje pri visokotemperaturno odpornih jeklih

1 Introduction

In the metallurgy of iron and steels many phenomena and processes, such as carburization/decarburization, nitrogenation/denitrogenation, corrosion, surface diffusion, sintering, recrystallization, adhesion, friction, wear, etc. are determined decisively by the atomic composition of the surface. Also the atomic composition of the grain boundaries is very important in affecting the mechanical properties and the corrosion behavior of steels. These interfaces will normally be covered with impurity atoms from the gas phase or segregation of dissolved atoms from the bulk, and also the grain boundaries by segregation from the bulk.

The equilibrium segregation on iron surfaces and at grain boundaries

$$\text{A(dissolved)} = \text{A(segregated)} \qquad (1)$$

where A = C, Si, Sn, N, P, O, S... has been investigated for binary systems Fe-A by surface analytical methods. Concentrations of the extraneous elements on the surface were determined by Auger-Electron-Spectroscopy (AES) in dependence on the bulk concentration x_A and on the temperature of equilibration, and ordered structures on surfaces were determined by LEED[1–7] i.e. Low Energy Electron Diffraction. The binding modes were characterized by X-ray photoelectron spectroscopy (XPS)[8–14].

Impurities in steels can have strong effects on the mechanical properties and on the corrosion behavior, especially if they tend to enrich at the grain boundaries. Sn, P, As, Sb, S, Se, and Te segregate at grain boundaries and embrittle steels. The study of this segregation, which is restricted to a few monolayers in the interface, was possible since the development of AES. By fracture of specimens inside an UHV chamber and by AES-analysis of the intergranular fracture faces, grain boundary concentrations of the embrittling elements could be determined. In our studies, grain boundary segregation of C, N, and B was also detected. These elements are not embrittling and, therefore, their detection is possible only if an embrittling element such as S or P is present which initiates intergranular fracture. In our AES-investigations on different steels mainly the impurity elements P and Sn were detected at grain boundaries. Obviously, other impurities such as As and Sb are present only in too small bulk concentrations, and sulfur is being scavenged by Mn so that the studies have been focused on the grain boundary segregation of P and Sn in iron, and on the effects of P and Sn on materials properties[15–30].

The equilibria were studied of grain boundary segregation of P and Sn in binary Fe-P and Fe-Sn, ternary, and quaternary alloys, by equilibrating specimens at different temperatures for sufficient time, afterwards analyzing intergranular fracture faces by AES.

The thermodynamics of segregation as well for surface segregation and for grain boundary segregation are described by the Langmuir-McLean equation:

$$\Theta_i/(1-\Theta_i) = x_i \exp(-\Delta G_i^o/RT) \qquad (2)$$

where

Θ_i: the occupancy of the grain boundary sites with the segregating element i

x_i: the mole fraction in the bulk.

The free energy of segregation is

$$\Delta G_i^o = \Delta H_i^o - T\Delta S_i^{xs} \qquad (3)$$

where

ΔH_i^o: the enthalpy of segregation

ΔS_i^{xs}: the excess entropy of segregation.

According to thermodynamics the segregation increases with decreasing temperature and with increasing bulk concentration.

All investigations of the surface segregation have been performed in the temperature and concentration range of the α- or γ-solid solution, in order to avoid the formation of three-dimensional compounds. Also the equilibria of grain boundary segregation have been established at elevated temperature within this range of the phase diagram and were measured on rapidly quenched specimens.

In the following some examples are presented of studies on the surface segregation of C, Si, Sn, O and S which demonstrate the principles of segregation thermodynamics and structures. Studies on grain boundary segregation are described of P and Sn. The results of the segregation studies are correlated to metallurgical phenomena, such as the effect of S on surface reactions, the effect of Sn on creep of heat resistant steels and the effects of P by grain boundary embrittlement and in corrosion.

2 Surface Segregation

2.1 Carbon

The surface segregation of carbon has been investigated in the temperature range 400–800°C on single crystals with carbon concentrations between 10 to 100 ppm C[1–3]. On Fe(100) a c(2 × 2) structure (**Fig. 1**) with 50 at% C is approached for high concentrations and low temperatures, this is the saturation coverage (Θ = 1). The degree of coverage Θ decreases with increasing temperature and decreasing bulk concentration, as expected from thermodynamics, see **Fig. 2.** These dependencies are described by the Langmuir-McLean equation (2). This equation can be rewritten according to

$$\ln \frac{\theta_i}{1-\theta_i} = \frac{-\Delta H_i}{RT} + \frac{\Delta S_i^{xs}}{R} + \ln x_i \qquad (4)$$

For the case of carbon on Fe(100) the segregation enthalpy is - 85kJ/mol, as derived from the plot according to Eq. (4) shown in **Fig. 3.** Thus the segregation of carbon is strongly exothermic, which is caused by the elastic energy which is set free when the carbon atom can leave the too narrow interstitial sites in the lattice and pops up to the surface[1].

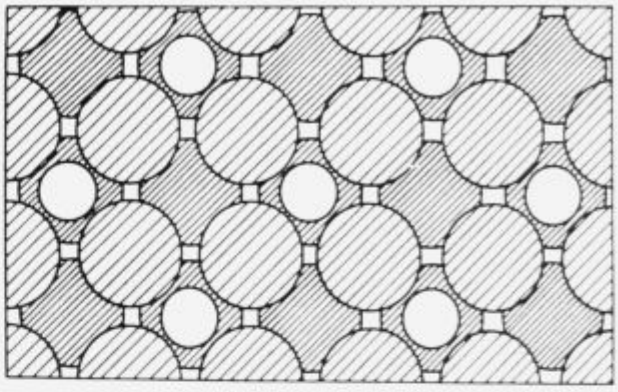

a)

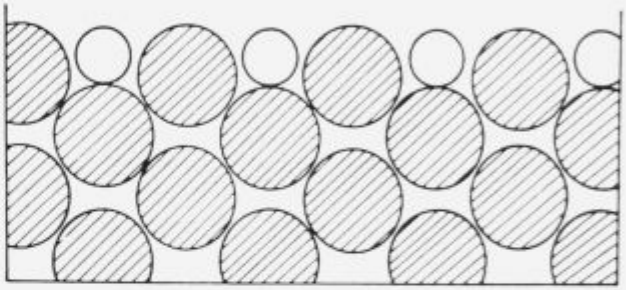

b)

Figure 1. Model of the c(2 × 2) adsorption structure of carbon on the Fe(100) surface, derived from LEED studies a) top view b) cross section in (110) direction

Slika 1. Model c(2 × 2) adsorpcijske strukture ogljika na površini Fe(100), dobljen s pomočjo LEED raziskav a) pogled z vrha b) presek v smeri (110)

For carbon segregation on other orientations of iron, the results are not so simple and clear[3].

The binding mode of carbon on Fe(100) has been characterized by photoelectron spectroscopy (XPS)[12]. Spectra from single crystal surfaces with segregated C have been taken and have been compared with spectra of graphite and cementite $(Fe,Cr)_3C$. (In order to obtain a thermodynamically stable cementite a Fe-2%Cr alloy had been carburized in $CH_4 - H_2$). The photolines of the C 1s photoelectrons of carbon are shown in **Fig. 4.**

The sample with 20 ppm C only shows the peak for segregated carbon, on the sample with 40 ppm C besides segregated carbon there is graphite deposited by oversaturation (at 600°C). The energies of the C 1s electron levels are distinctly different from the energy level of C 1s in graphite and in the carbide. The segregated carbon is a special state of carbon. The shift of energy, about −2.0 eV in comparison to graphite, indicates that a certain electron transfer has taken place from iron to carbon. The bond Fe-C is similar as in cementite, prevailing homopolar, but it is somewhat stronger polarized than in the carbide.

2.2 Silicon

The surface segregation of Si has been studied on Fe-3%Si single crystals in the temperature range 450–900°C[6]. The dependence of surface concentration on temperature has been measured for the equilibrium of silicon segregation

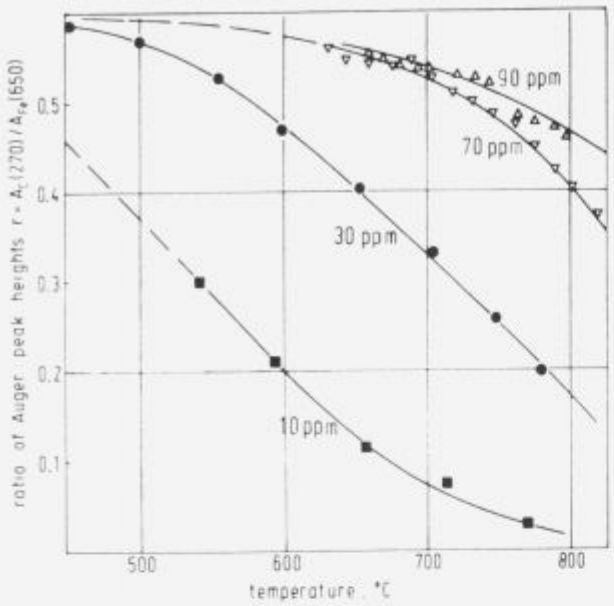

Figure 2. Equilibrium segregation of carbon on Fe(100), AES measurements of the surface concentration of carbon on samples with different bulk concentration in dependence on temperature
Slika 2. Ravnotežna segregacija ogljika na površini Fe(100), AES meritve koncentracije ogljika na površini vzorcev z različno koncentracijo v masivnem materialu, v odvisnosti od temperature

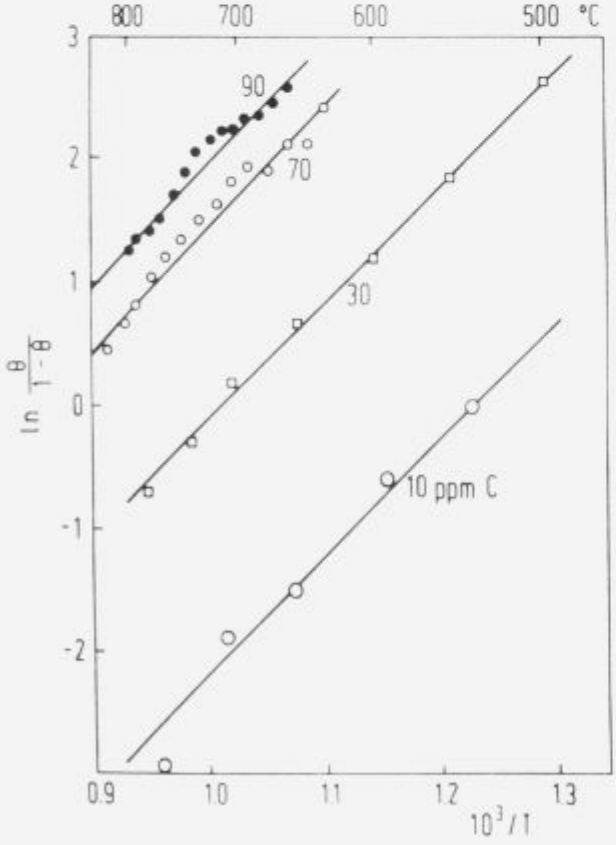

Figure 3. Plot of the data in Fig. 2 on equilibrium segregation of carbon on Fe(100) according to the Langmuir-McLean equation
Slika 3. Grafični prikaz podatkov s slike 2, ravnotežne koncentracije ogljika na površini Fe(100) v skladu z enačbo Langmuir-McLean

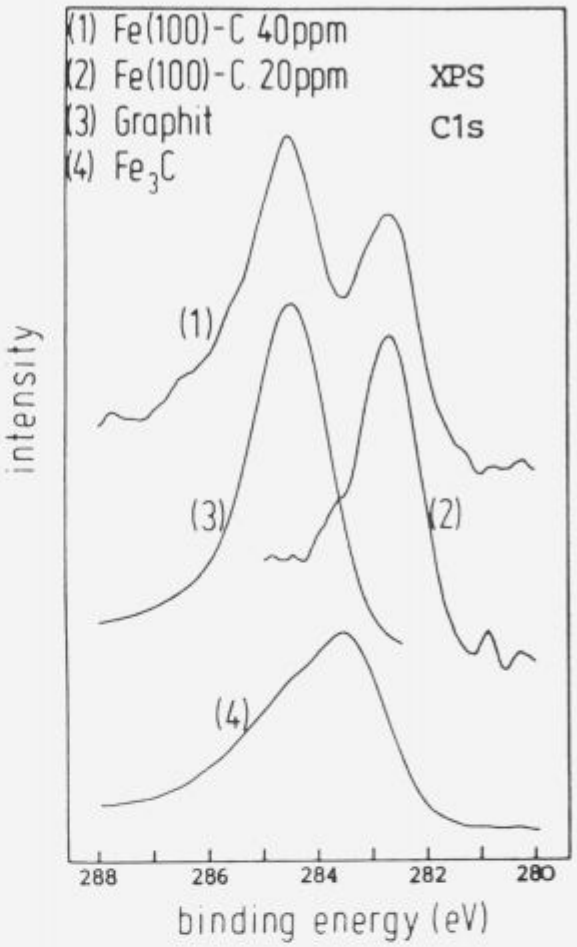

Figure 4. Investigations of the binding of carbon by photoelectron spectroscopy (XPS) (1) segregated carbon and graphite on Fe(100) (2) segregated carbon on Fe(100) (3) graphite (4) carbon in cementite $(Fe, Cr)_3C$
Slika 4. Raziskave vezave ogljika z metodo XPS (1) segregirani ogljik in grafit na površini Fe(100) (2) segregirani ogljik na površini Fe(100) (3) grafit (4) ogljik in cementit $(Fe, Cr)_3C$

on Fe(100). This dependence can be described by the Langmuir-McLean equation (2). The result for the Gibbs' free energy of segregation is

$$\Delta G^{\circ} = -48\,000 + 15T \text{ (J/mol)} \qquad (5)$$

The value of the segregation enthalpy of silicon on iron $\Delta H^{\circ}_{Si} = -48$ kJ/mol is much lower than for carbon. Thus carbon can displace silicon from the surface on Fe-3%Si samples which contain small concentrations of carbon:

$$\text{C(dissolved)} + \text{Si(segregated)} = \text{C(segregated)} + \text{Si(dissolved)} \qquad (6)$$

This equilibrium of mutual displacement has been measured in dependence on temperature, see **Fig. 5.**

According to the higher value for ΔH°_{C} the C-segregation prevails at lower temperatures, for higher temperatures the carbon segregation decreases and silicon is able to segregate to the surface. This equilibrium was described by equations which consider the site competition of both segregating elements:

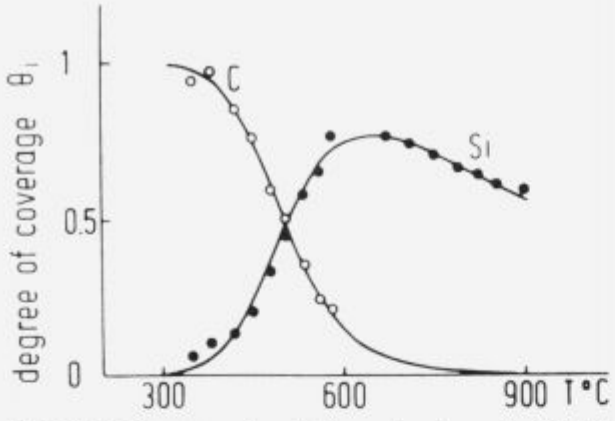

Figure 5. Surface segregation of silicon and carbon on Fe-3%Si(100) with 40 ppm carbon, mutual displacement of carbon and silicon in dependence on temperature

Slika 5. Segregacija silicija in ogljika na površini Fe-3%Si(100) z 40 ppm ogljika, vzajemna zamenjava ogljika in silicija v odvisnosti od temperature

$$\Theta_{Si}(1 - \Theta_{Si} - \Theta_C) = x_{Si} \exp(-\Delta G^o_{Si}/RT) \quad (7)$$

$$\Theta_C(1 - \Theta_C - \Theta_{Si}) = x_C \exp(-\Delta G^o_C/RT) \quad (8)$$

Here the thermodymic values for the Si-segregation stay unchanged, while the value for ΔH^o_C is increased by the presence of Si.

2.3 *Tin*

The surface segregation of tin was investigated on (100) faces of Fe-4%Sn samples in the temperature range 600–800°C[7]. During segregation of tin at 600°C by diffusion there is a step in the increase of concentration with time, see Fig. 6a which can be associated with the formation of the saturated c(2 × 2) structure. However, the surface concentration continues to increase till a coverage of about 1.2 tin atoms per iron atoms is obtained. During this process the LEED-diffraction pattern vanishes, obviously a change of the surface structure occurs from the ordered structure to disorder. In this transition the binding mode of the segregated tin changes, as can be seen from the photolines. The binding energies of the electrons in the Sn 3d and Fe 2p levels show distinct changes in the transition. The d-levels of the segregated tin shift in the direction to the values determined for pure tin. At the lower surface concentration of tin the binding energies of the electrons are lower, this may be interpreted similar as in the case of carbon by an electron transfer from iron to the tin atoms in the ordered c(2 × 2) structure. A tentative phase diagram is drawn in Fig. 6b, with saturated surface structures at $\Theta = 0.5$ and 1.2 and heterogeneous regions in between. A similar phase transition as on Fe(100) is observed also on Fe(111), while different complex ordered structures are observed on Fe(110) with increasing degree of coverage[7]. The tendency for surface segregation is very high for tin, trials with different small concentrations always led to high surface concentrations $\Theta > 1$, which means that no thermodynamic data could be obtained but the segregation enthalpy of tin must be a rather high negative value.

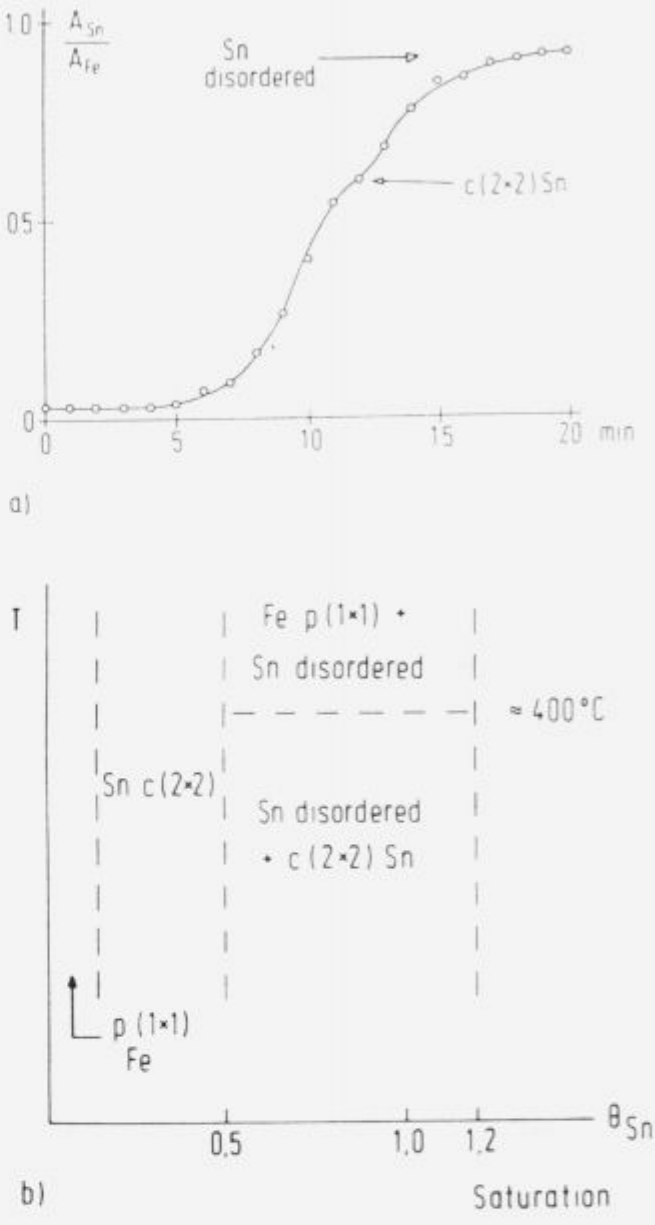

Figure 6. Surface segregation of tin on Fe-4%Sn(100) a) Kinetics of Sn segregation, measurement of the Auger peak ratio A_{Sn}/A_{Fe} after heating from room temperature to 600°C (in 6 min), after about 12 min c(2 × 2) structure with 50 at% coverage as demonstrated by LEED diffraction pattern b) "Phase diagram" of the system Sn on Fe(100), stability ranges of the surface phases in dependence on temperature and degree of coverage

Slika 6. Segregacija kositra na površini Fe-4%Sn(100) a) kinetika segregacije kositra, meritve razmerja Augerjevih vrhov A_{Sn}/A_{Fe} po žarjenju od sobne temperature do 600°C (v 6 minutah), po približno 12 minutah c(2 × 2) strukture s 50% prekritjem, prikazano z LEED difrakcijskim modelom b) "Fazni diagram" sistema Sn na Fe(100), stabilna območja površinskih faz v odvisnosti od temperature in stopnje prekritja

2.4 *Oxygen*

The surface segregation of oxygen on iron cannot be investigated with the segregation method described before, since the oxygen solubility in iron is very small. In spite of

that, segregation equilibria can be established, even at well-defined thermodynamic potential of the oxygen if a solid electrolyte cell is used: iron sample/oxygen-ion conducting solid electrolyte/reference electrode. Such cell, for example $Fe/ThO_2 \times Y_2O_3/Cr - Cr_2O_3$, can be inserted into a UHV system, and by controlling the cell voltage the chemical potential of oxygen can be fixed in and on the sample. Thus, the oxygen segregation at a certain oxygen potential is established. With this set-up measurements are possible at oxygen potentials, which correspond to oxygen pressures in the range 10^{-40}–10^{-10} atm. **Fig. 7** shows an example of a measurement of the oxygen segregation on an iron film, vapour deposited on the solid electrolyte. A two-step isotherm is observed, obviously there are two adsorption structures, at $> 10^{-35}$ bar O_2 with the ratio O/Fe = 0.25 and at $> 10^{-25}$ bar with the ratio O/Fe = 1. The oxygen adsorption at very low oxygen pressures $< 10^{-35}$ bar O_2 can be related to oxygen adsorbed on steps, kinks, and other active sites of the surface. LEED and AES studies with iron single crystals[5], which had been sintered together with a mixture of Fe and the lowest oxide FeO, showed a p(1 × 1) structure at 800°C on Fe(100). This is in agreement with the degree of coverage O/Fe = 1 for oxygen pressures near the equilibrium Fe-FeO. Oxygen on Fe(100) is also embedded in central sites between four iron atoms[13], however, in contrast to the other nonmetal atoms it reaches not only 50% coverage in a c(2 × 2) structure but 100% coverage in p(1 × 1). The oxygen adsorption and oxide nucleation can be depicted as shown in **Fig. 8.**

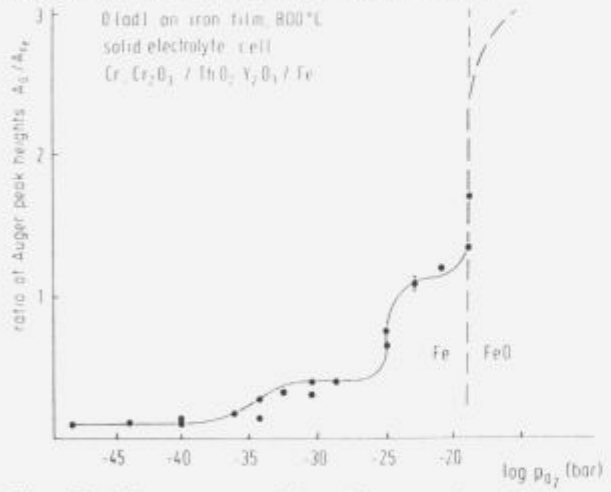

Figure 7. AES measurement of the surface segregation of oxygen on an iron film and of the oxidation to FeO, the oxygen potential is established by the solid electrolyte cell Cr, $Cr_2O_3/ThO_2 - Y_2O_3$/Fe

Slika 7. AES meritve segregacije kisika na površini tanke plasti železa in oksidacije do FeO, kisikov potencial je bil določen s pomočjo trdne elektrolitske celice Cr, $Cr_2O_3/ThO_2 - Y_2O_3$/Fe

2.5 *Sulfur*

Sulfur is extremely "surface active" on iron surfaces, even for very small bulk concentrations < 1 ppm in the stability range of the α-phase up to 900°C always saturation of the surface with sulfur was observed after equilibration[2]. The presence of sulfur on the iron surface strongly affects surface reaction kinetics in the case of carburization and nitrogenation of iron[2,4] and also the surface diffusion is influenced by adsorbed sulfur, the surface self-diffusivity of iron is enhanced in the presence of adsorbed sulfur[32].

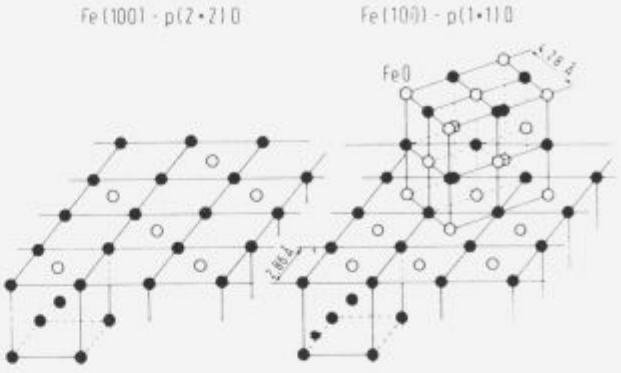

Figure 8. Model of oxygen adsorption and oxide nucleation on Fe(100) a) Adsorption structure p(2 × 2) b) Adsorption structure p(1 × 1) and FeO nucleation

Slika 8. Model adsorpcije kisika in nukleacija oksida na površini Fe(100) a) Adsorpcijska struktura p(2 × 2) b) Adsorpcijska struktura p(1 × 1) in nukleacija FeO

On Fe(100) the c(2 × 2) structure is obtained, up to high temperatures a very distinct LEED pattern of this structure can be observed. **Fig. 9** shows this adsorption structure of segregated sulfur which was proved by measurements and theoretical calculations of the LEED intensity energy curves. In this schematic the diameter of sulfur is assumed to be equal to the diameter of S^{2-} ions. It is obvious that such dense coverage with sulfur ions will strongly retard any surface reactions, this is demonstrated in **Fig. 10** for the carburization of iron in $CH_4 - H_2$ and the nitrogenation in N_2. For these reactions the rate was determined in resistance relaxation measurements in flowing gas mixtures (at 1 bar), in many experiments, in which the sulfur activity was given by the $H_2S - H_2$ ratio in the atmosphere[4,32].

Determinations of the electron levels of segregated sulfur by photoelectron spectroscopy[10] confirmed that these are very near to the electron levels of the doubly-ionized sulfur ion S^{2-}. The binding energy of the S 2p and S 2s electrons is by some 10th of an eV higher than in the sulfides FeS and FeS_2.

In steels the surface segregation of sulfur is somewhat reduced by the presence of Mn, the sulfur is tied up in MnS, its solution concentration and therefore its surface concentration is descreased.

3 Grain Boundary Segregation

3.1 *Grain Boundary Segregation of Phosphorus in Ferrite and Austenite*

3.1.1 Ferrite

The equilibrium grain boundary segregation of P in ferrite was studied on 7 Fe-P melts with P contents in the range 0.003 to 0.33 wt% P[17]. As expected, according to thermodynamics, the grain boundary concentration decreases with increasing temperature and with decreasing bulk concentration, **Fig. 11,** and the data could be evaluated according to the Langmuir-McLean equation (4). The free enthalpy of grain boundary segregation of phosphorus in α-iron can be written:

$$\Delta G_P^o = -34\,300 - 21.5T \text{ (J/mol)} \qquad (9)$$

The presence of phosphorus in the grain boundaries induces grain boundary embrittlement, with increasing grain

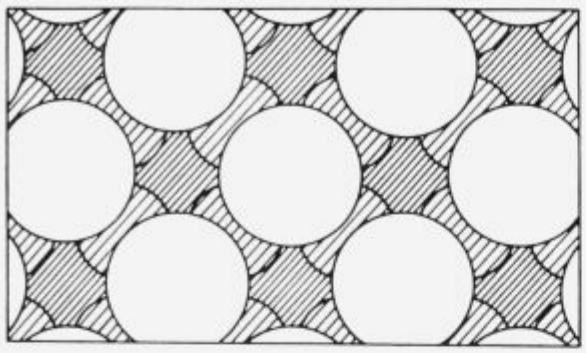

a)

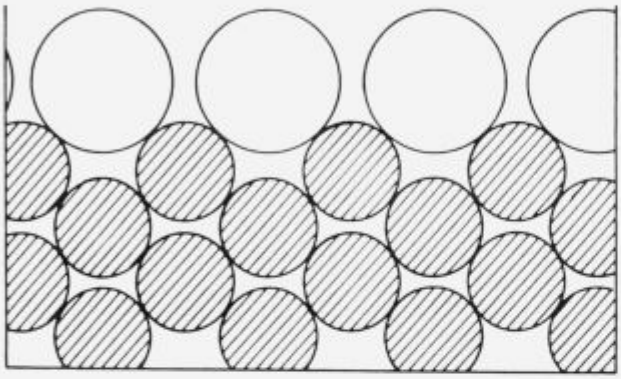

b)

Figure 9. Model of the c(2 × 2) adsorption structure of sulfur on the Fe(100) surface, derived form LEED studies a) top view and b) cross section in (110) direction

Slika 9. Model adsorpcijske strukture c(2 × 2) žvepla na površini Fe(100), dobljen s pomočjo LEED raziskav a) pogled z vrha in b) presek v smeri (110)

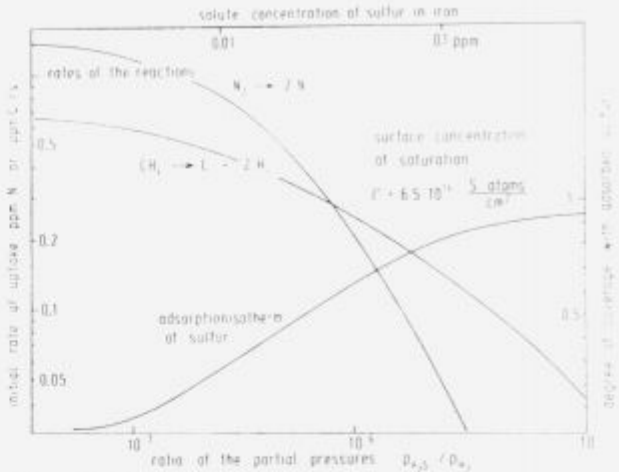

Figure 10. Effect of sulfur on the rate of carburization and rate of nitrogenation, initial rates measured using the resistance-relaxation method in flowing gas mixtures $CH_4 - H_2 - H_2S$ or $N_2 - H_2 - H_2S$ at 1 bar, in dependence on the sulfur activity given by the ratio H_2S/H_2 in the gas mixtures. The diagram also shows the adsorption isotherm of sulfur on iron at the reaction temperature 850°C derived from the kinetic measurements

Slika 10. Vpliv žvepla na stopnjo naogljičenja in stopnjo nitriranja, začetne stopnje so bile izmerjene ob uporabi uporovnorelaksacijske metode v toku plinske mešanice $CH_4 - H_2 - H_2S$ ali $N_2 - H_2 - H_2S$ pri 1 bar, v odvisnosti od aktivnosti žvepla, ki je podana z razmerjem H_2S/H_2 v plinski mešanici. Diagram prikazuje tudi adsorpcijsko izotermo žvepla na železu pri reakcijski temperaturi 850°C, dobljeno pri meritvah kinetike

boundary phosphorus concentration the fracture mode (at low temperatures) changes from transgranular to intergranular, see **Fig. 12.**

In a similar way the grain boundary segregation in Fe-C-P alloys was investigated[17]. Different concentrations in the range 10 to 100 ppm C were introduced to specimens with constant bulk concentrations of P by carburization in $CH_4 - H_2$ mixtures. The specimens were annealed at different temperatures to establish the equilibrium grain boundary segregation of C and P, quenched and analyzed by AES. The results indicate displacement of phosphorus by carbon at the grain boundaries, according to

$$\text{C(dissolved)} + \text{P(segregated)} = \text{C(segregated)} + \text{P(dissolved)} \qquad (10)$$

With increasing carbon content the grain boundary concentration of phosphorus decreases and the grain boundary concentration of carbon increases, see **Fig. 13.** At 600°C the solubility limit of carbon is about 55 ppm, at higher concentrations cementite precipitates and no further changes of grain boundary concentrations are to be expected.

The increasing carbon concentration in the bulk and in the grain boundaries causes a decrease in the percentage of intergranular fracture, thus carbon acts as a de-embrittling element. The displacement of phosphorus and carbon according to Eq. (10) can be described by equations considering the site competition of both elements.

$$\Theta_P/(1 - \Theta_P - \Theta_C) = x_P \exp(-\Delta G_P^\circ/RT) \qquad (11)$$

$$\Theta_C/(1 - \Theta_P - \Theta_C) = x_C \exp(-\Delta G_C^\circ/RT) \qquad (12)$$

From more extensive investigations[29] in this system also the Gibbs' free energy could be determined for grain boundary segregation of carbon in ferrite which is -72 kJ/mol at 500°C compared to -49 kJ/mol for phosphorus. This description of the displacement equilibrium (11) at grain boundaries corresponds to the result for the displacement equilibrium of carbon and silicon on the iron surface, see Eqs. (6) to (8).

In carbon steels with carbon contents higher than the maximum solubility in ferrite (0.02% at 735°C) the carbon concentration is given by equilibrium with cementite and is relatively high in the critical temperature range concerning phosphorus segregation, thus grain boundary segregation in carbon steels generally will be low. However, the addition of carbide-forming elements, e.g. some percents of Cr or Mn, decreases the solubility of carbon, therefore the equilibrium (10) is shifted to higher grain boundary segregation of phosphorus, see Fig. 14. This effect is not caused by direct interaction of Cr or Mn with P, by some "synergistic cosegregation" as assumed by other authors,[33,34] but by the reduction of carbon concentration in bulk and grain boundaries in the presence of $(Fe,Cr)_3C$ respectively $(Fe,Mn)_3C$, whereby phosphorus can segregate to the grain boundaries. **Fig. 14** demonstrates these results, grain boundary segregation in carbon-free alloys Fe-P and Fe-Cr-P is the same and unaffected by the presence of Cr, grain boundary seg-

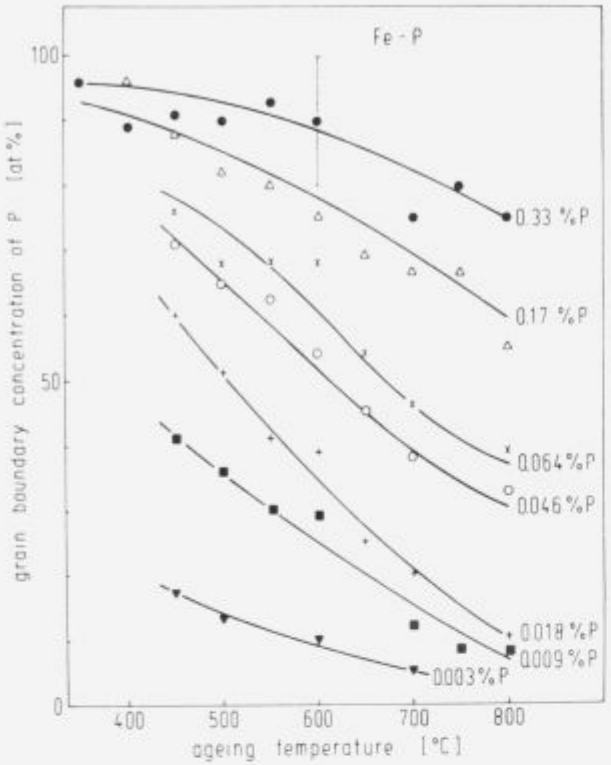

Figure 11. Grain boundary concentrations of phosphorus determined by AES in Fe-P alloys of different P contents, plotted vs the equilibration temperature

Slika 11. Koncentracija fosforja na mejah zrn, določena z metodo AES v Fe-P zlitinah z različno vsebnostjo fosforja, grafično prikazana v odvisnosti od ravnotežne temperature

regation in Fe-Cr-C-P, however, is considerably increased compared to Fe-C-P[17,35].

3.1.2 Austenite

Grain boundary segregation of P in austenite was investigated after annealing of samples in the austenitic range and quenching in water[25,30–32]. The evaluation of data obtained with binary alloys containing 0.09, 0.145, and 0.20% P yielded a value of $\Delta G_P^\circ = -49 \pm 4$ kJ/mol at 1000°C, similar as for ferrite at 500°C. Thus, the grain boundary concentrations are considerable, between 15–30 at% of a monolayer for these alloys, see **Fig. 15.** As to be expected, the grain boundary concentration decreases with increasing temperature. Also in austenite the presence of carbon decreases grain boundary segregation of P and Eqs. (11) and (12) can be applied, the free energy of grain boundary segregation can be derived for carbon in austenite to be

$$\Delta G_C^\circ = -30 \text{ kJ/mol}.$$

The effect of boron on phosphorus segregation in austenite is similar to the effect of carbon but much more pronounced. Even very small concentrations of boron in the range 5 to 30 ppm B strongly decrease the phosphorus segregation. Boron also was detected at the austenite grain boundaries[30], its free energy of grain boundary segregation is relatively high, $\Delta G_B^\circ \approx -100$ kJ/mol.

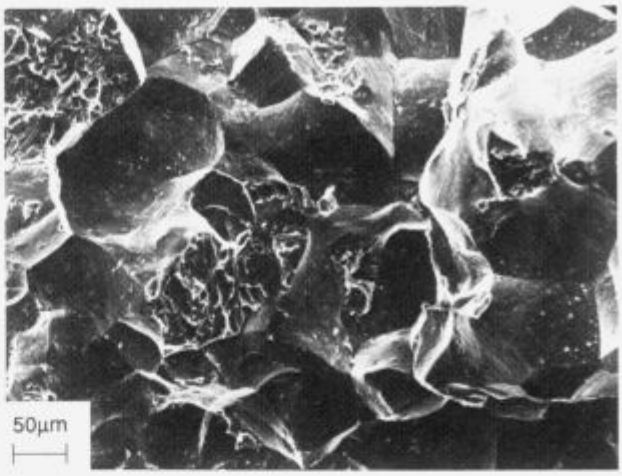

a)

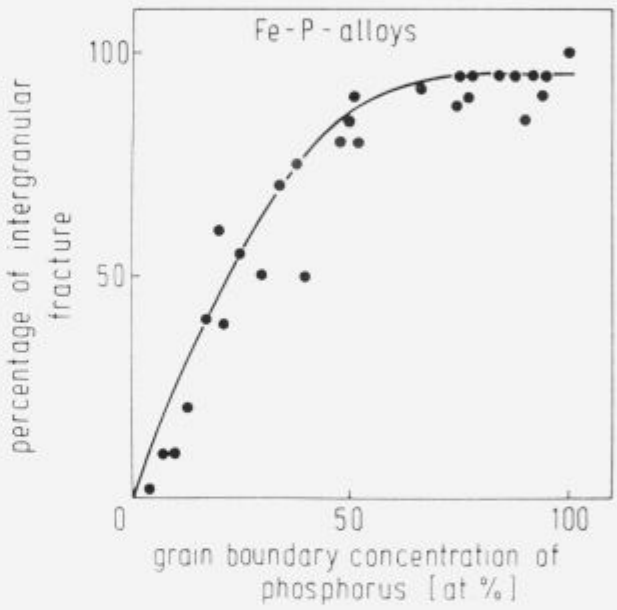

b)

Figure 12. Intergranular fracture caused by P grain boundary segregation a) Fracture face of sample with high grain boundary concentrations of phosphorus, fractured in the UHV system by impact at about -100°C b) the percentage of intergranular fracture is clearly related to the grain boundary concentration

Slika 12. Interkristalni prelom povzročen zaradi segregacije P po mejah zrn a) Prelomne ploskve vzorca z visoko vsebnostjo fosforja, ki je segregiral po mejah zrn; vzorec je bil prelomljen v UVV pri temperaturi okrog -100°C b) odstotek interkristalnega preloma je v vidni povezavi s koncentracijo na mejah zrn

3.2 Grain Boundary Segregation of Tin in Ferrite

For a study of the equilibrium grain boundary segregation of tin, 7 Fe-Sn melts were prepared with tin contents in the range 0.02 to 0.2 wt% Sn[26]. The scatter of the measured values is very large, possibly due to a strong orientation dependence of tin grain boundary segregation, see **Fig. 16.** However, the average values could be fitted with the Langmuir-McLean equation (2), the values were obtained

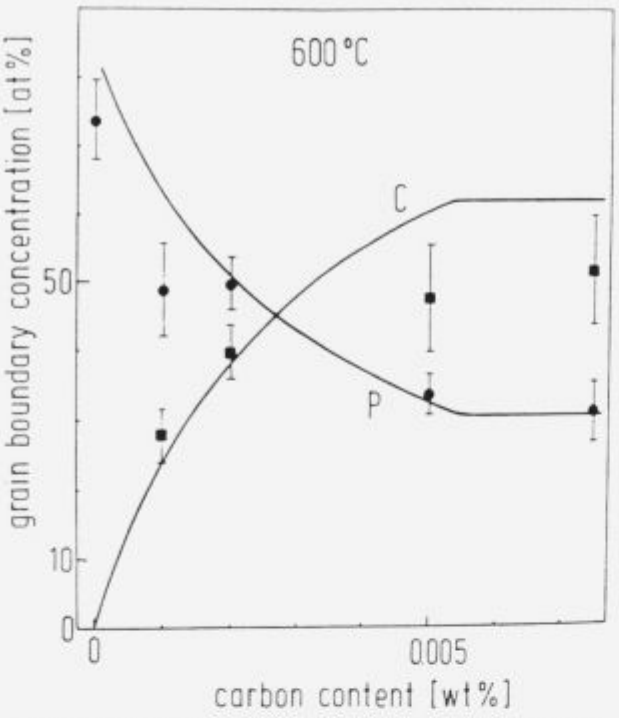

Figure 13. Grain boundary concentrations of phosphorus and of carbon in Fe-0.17%P at different carbon concentrations. Dependence of grain boundary concentrations on the bulk carbon concentration after equilibration at 600°C

Slika 13. Koncentracija fosforja in ogljika na mejah zrn v Fe-0.17% P pri različnih vsebnostih ogljika. Odvisnost koncentracije na mejah zrn od vsebnosti ogljika v masivnem materialu po doseženem ravnotežju pri 600°C

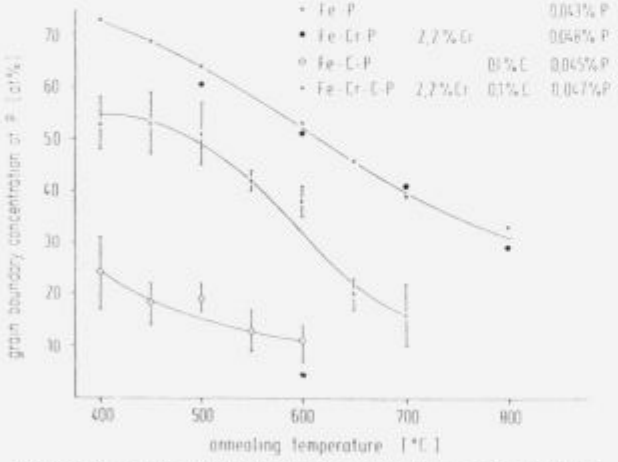

Figure 14. Effects of carbon and chromium on the grain boundary segregation of phosphorus in Fe-P, Fe-Cr-P, Fe-C-P, and Fe-Cr-C-P alloys with about the same P concentration in dependence on the equilibration temperature

Slika 14. Vpliv ogljika in kroma na segregacijo fosforja po mejah zrn v Fe-P, Fe-Cr-P, Fe-C-P in Fe-Cr-C-P zlitinah s približno enako vsebnostjo P v odvisnosti od ravnotežne temperature

for the free energy of segregation.

$$\Delta G^{\circ}_{Sn} = -(22\,500 \pm 2\,800) - (26.1 \pm 0.9)T \text{ (J/mol)} \quad (13)$$

These data indicate a rather low tendency to grain boundary segregation of tin.

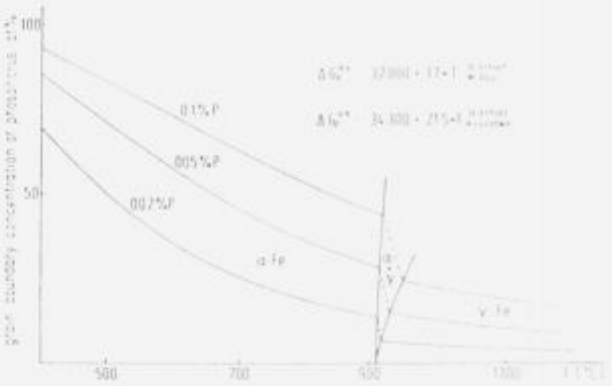

Figure 15. Grain boundary segregation in ferritic and austenitic Fe-P alloys calculated according to Ref. 17 and 30

Slika 15. Segregacija po mejah zrn v feritnih in avstenitnih Fe-P zlitinah, izračunanih v skladu z ref. 17 in 30

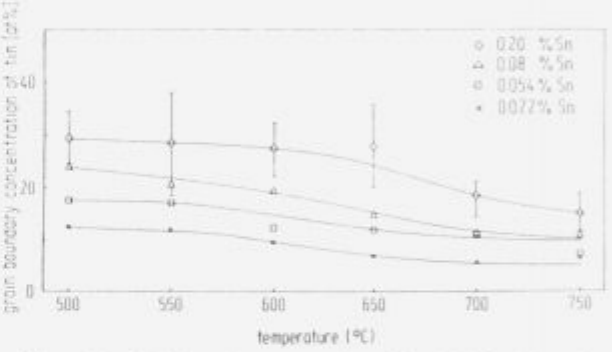

Figure 16. Grain boundary segregation of tin in Fe-Sn alloys of different Sn content in dependence on temperature

Slika 16. Segregacija kositra po mejah zrn v Fe-Sn zlitinah z različno vsebnostjo Sn, v odvisnosti od temperature

Furthermore, tin can be displaced by carbon from grain boundaries. With increasing carbon content in Fe-Sn-C alloys the tin concentration at the grain boundaries decreases and the carbon concentration at the grain boundaries increases, simultaneously the tendency to intergranular fracture is reduced.

According to these results there is no great danger of tin segregation to grain boundaries for most steels. According to thermodynamics in equilibrium with usual bulk concentrations ≤ 0.02 wt% Sn, the grain boundary concentration will be low, even small concentrations of dissolved and segregated carbon will keep the tin from the grain boundaries in carbon steels.

Furthermore, the diffusion of Sn in iron is slow, during usual processing and heat treatment of steels there will be no time for tin segregation to grain boundaries.

However, upon application of heat resistant steels at elevated temperatures $> 500°C$ effects of tin are expected which result less from grain boundary segregation but more from surface segregation in cavities, since the tendency to surface segregation is very high[7].

4 Effects on materials properties

4.1 Long-term embrittlement of a 3.5 NiCrMoV steel

For low pressure steam rotors NiCrMoV-steels are preferred since large rotors can be tempered and a good toughness is

achieved. However, these steels show a tendency to long-term embrittlement, therefore their use had to be restricted to temperatures about 350°C. A sufficient ductility must be retained during long-term application up to 250,000 h. The ductility is affected by the grain boundary segregation of phosphorus.

For prediction and control of embrittlement, the grain boundary segregation of phosphorus in the 3.5 NiCrMoV-steels was studied[24] and its effects on the ductility (transition temperature) of that steel. Two melts were prepared with 0.048% and 0.10% P, samples were annealed at temperatures between 400 to 500°C for different times and then the grain boundaries were analyzed by AES. The grain boundary concentration of phosphorus approaches equilibrium, as shown in **Fig. 17.** The curves can be fitted applying McLean's equation for diffusion-controlled segregation and the Langmuir-McLean equation for describing the equilibrium. The diffusivities of P are given by

$$D = 0.13^{-3} \exp(-176\ \mathrm{kJ/mol}^{-1}/RT)$$

and the Gibbs' free energy of equilibrium segregation

$$\Delta G^{\circ} = -46\,350 + 0.5T\ (\mathrm{J/mol})$$

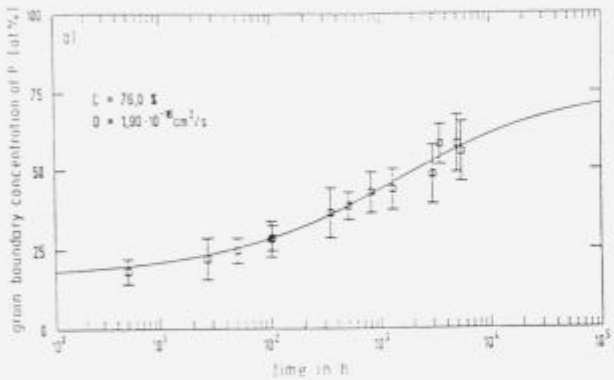

Figure 17. Kinetics of the grain boundary segregation of P in 3.5% NiCrMoV steel 0.048% P at 400°C. The curve is fitted using the values of equilibrium grain boundary concentration C and diffusion coefficient of phosphorus D, given in the diagram

Slika 17. Kinetika segregacije fosforja po mejah zrn v 3.5% NiCrMoV jeklu z 0.048% P pri temperaturi 400°C. Krivulja je dobljena z uporabo vrednosti ravnotežne koncentracije ogljika na mejah zrn in difuzijskega koeficienta fosforja D, danega v diagramu

With these data the grain boundary concentrations of P in the 3.5 NiCrMoC-steel were calculated for different bulk concentrations, in dependence on temperature and time, see **Fig. 18.** Values calculated for low temperatures and low bulk concentrations are well in agreement with AES-analyses of long-time annealed samples.

The transition temperature from the notch impact test is linearly correlated to the grain boundary concentration, for this steel the relation is $\Delta TT/\Delta c = 6.3$ (K/at% P). Using these data the change in transition temperature can be calculated for a steel of known phosphorus concentration which occurs during its application time and it can be decided if the application temperature may be raised.

For a steel with the bulk concentration 50 ppm P after 10^5 h at 400°C an increase of 19 at% in grain boundary concentration can be predicted which corresponds to an increase of transition temperature by about 120 K. At 350°C

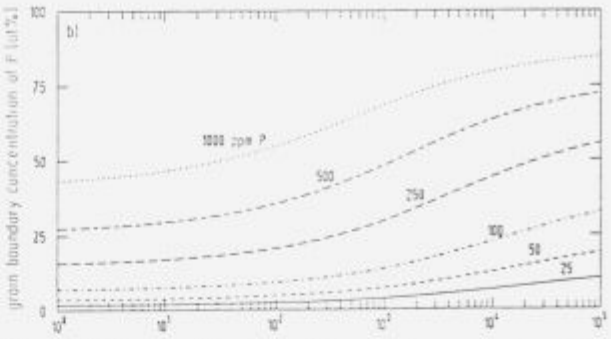

Figure 18. Curves calculated for different bulk concentrations of P, predicting the grain boundary segregation of P in 3.5% NiCrMoV steel during application at 400°C

Slika 18. Krivulje izračunane za različne koncentracije P v masivnem materialu za napovedovanje segregacije P v 3.5% NiCrMoV jeklu med uporabo pri temperaturi 400°C

the equilibrium concentration would be higher, but the diffusion is much slower, so the increase of grain boundary concentration is 13.5 at% P and $\Delta TT \approx 85$°C. Accordingly, such steel cannot be applied at 400°C, for that purpose the bulk concentration of P must be even lower (< 30 ppm).

Nowadays, "clean steels" are produced with ≤ 25 ppm of P which can be used at 400°C without risk of embrittlement for up to 10^5 h.

4.2 Effects of tin on the creep of a 1% CrMoNiV steel

The creep properties of heat resistant steels to some extent depend on purity. Fracture at low stress and after long creep life occurs by the formation and growth of cavities along grain boundaries, when these cavities coalesce they form an intergranular fracture path. The formation and growth of cavities are favored and accelerated by grain boundary and surface segregation. AES-analyses of creep samples after long-time creep tests at 550°C had shown P at grain boundaries and P and Sn in cavities[36]. The effect of P on creep was tested for a 1% CrMoNiV steel, additions of 0.06, 0.045 and 0.1% P caused an increase of creep rate in the primary and secondary stage of creep[37].

For elucidating the effect of tin, melts of the 1% CrMoNiV steel were prepared with 0.044, 0.022, 0.061 or 0.12 wt% Sn. The creep specimens were annealed at 550°C for 2000 to 5000 h to establish the grain boundary segregation equilibria which were attained with relatively low grain boundary concentrations in the range 5 to 10% of a monolayer. The creep of these materials was measured at 550°C and loads of 200, 250, and 300 MPa (= Nmm^{-2}). In the experiments at 200 and 250 MPa during 1200 h of creep range, however, the tertiary creep starts earlier and leads to premature failure of the tin-doped steels, the earlier the higher the tin content, **Fig. 19.**

Investigation of the creep samples after the tests showed cavity formation at the grain boundaries and the AES spectra showed considerable Sn concentrations in the cavited areas.

In many cavities also MnS particles were detected which play an important role in the nucleation of voids (**Fig. 20**).

Tin has a high tendency (very negative ΔG^0 for surface segregation[7], but much less tendency for grain boundary segregation. This also leads to enhanced nucleation

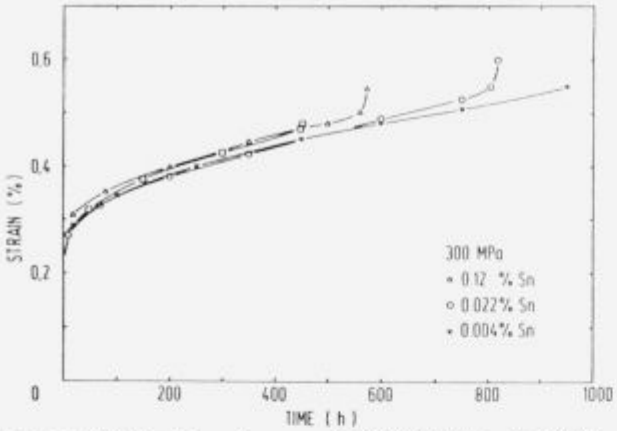

Figure 19. Effect of tin on the creep of 1% CrMoNiV steel at 550°C, creep curves at a load of 300 MPa for melts of different tin content
Slika 19. Vpliv kositra na lezenje 1% CrMoNiV jekla pri 550°C, krivulje lezenja pri obremenitvi 300 MPa za taline z različno vsebnostjo kositra

and growth rate of cavities. Thus, small concentrations of impurities such as Sn and S can strongly affect the creep properties and creep life of heat resistant steels.

4.3 Effects of phosphorus in stress corrosion cracking and hydrogen induced cracking of carbon steels

Carbon steels show intergranular stress corrosion cracking (IGSCC) in certain potential ranges upon corrosion in hot nitrate and hot hydroxide solutions. Cathodic polarization in sulphuric acid with and without arsenic causes hydrogen induced cracking (HIC). The resistance against IGSCC and HIC can be characterized by measuring the relative work of fracture in constant extension rate tests, i.e. the area below the stress-strain curves measured in the electrolyte related to the corresponding value measured in paraffin.

The effects of phosphorus on IGSCC and HIC were studied for steels with 0.15% and 0.4% or 2% Mn, the phosphorus contents were 0.003, 0.03 and 0.05% P[38,39]. Constant strain rate tests were conducted at constant potentials in 55% $Ca(NO_3)_2$ at 75°C, in 5N NH_4NO_3 at 75°C and 33% NaOH at 120°C. The strain rate was 10^{-6}/s. The grain boundary concentrations of phosphorus varied in dependence on bulk concentrations and heat treatment of the steel as determined by AES.

Tests in 5N NH_4NO_3 at 75°C at constant potential showed a decrease of resistance against IGSCC with increasing potential in the range -300 to 0 mV_H, in this range of potentials the work of fracture decreases with increasing P-content of the steels, **Fig. 21a**. At potentials 0 mV_H to 650 mV_H the resistance against IGSCC is very low for all steels, independent of P-content. In this range of potentials the grain boundaries are attacked already without load and the failure is by stress-assisted intergranular corrosion. At even higher potentials > 650 mV_H intergranular corrosion occurs without any load, iron in nitrate disintegrates into grains[16].

The behavior in 55% $Ca(NO_3)_2$ solution at 75°C is similar as in NH_4NO_3, however, the steels are resistant against IGSCC up to -100 mV_H. The decrease of work of fracture is observed in the potential range from −100 to +100 mV_H, the values being lower for the high phosphorus steels, see **Fig. 21b.** At higher potentials the resistance against IGSCC is again very low and independent of P-content.

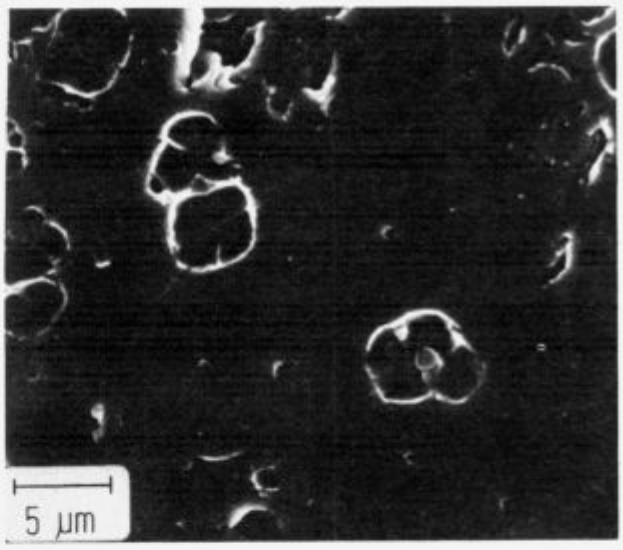

a)

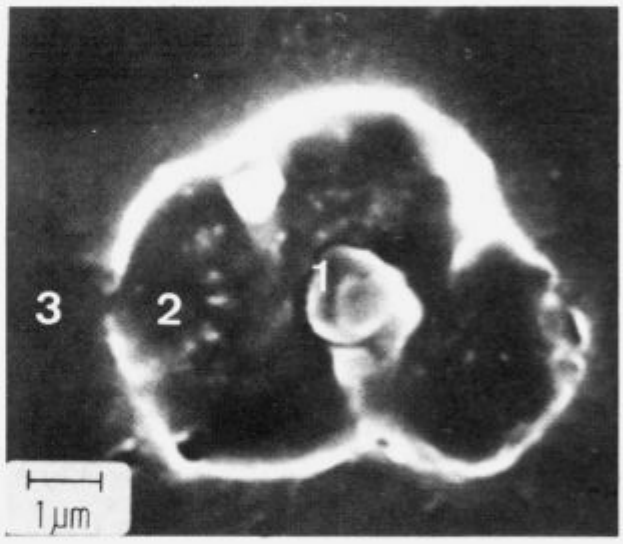

b)

Figure 20. Cavity formation in the fracture surface of steel with 0.061% Sn after a creep test at 300 MPa for 498 h a) SEM-photo of a fracture face with several creep cavities b) SEM-photo of a cavity with an MnS particle in the middle, points are indicated where AES spectra have been taken
Slika 20. Tvorba por na prelomni površini jekla z 0.061% Sn po testu lezenja pri 300 MPa in po 498 urah a) SEM posnetek prelomne površine s številnimi porami, ki so nastale zaradi lezenja b) SEM posnetek pore z MnS vključkom v sredini, označena so mesta, kjer so bili posneti AES spektri

The effect of phosphorus on the IGSCC is caused by P-segregated at grain boundaries, with increasing grain boundary concentration of P the steels become less resistant. The grain boundary concentration is low for steels after normalizing and quenching, the grain boundary concentration increases upon holding the steels at 500°C.

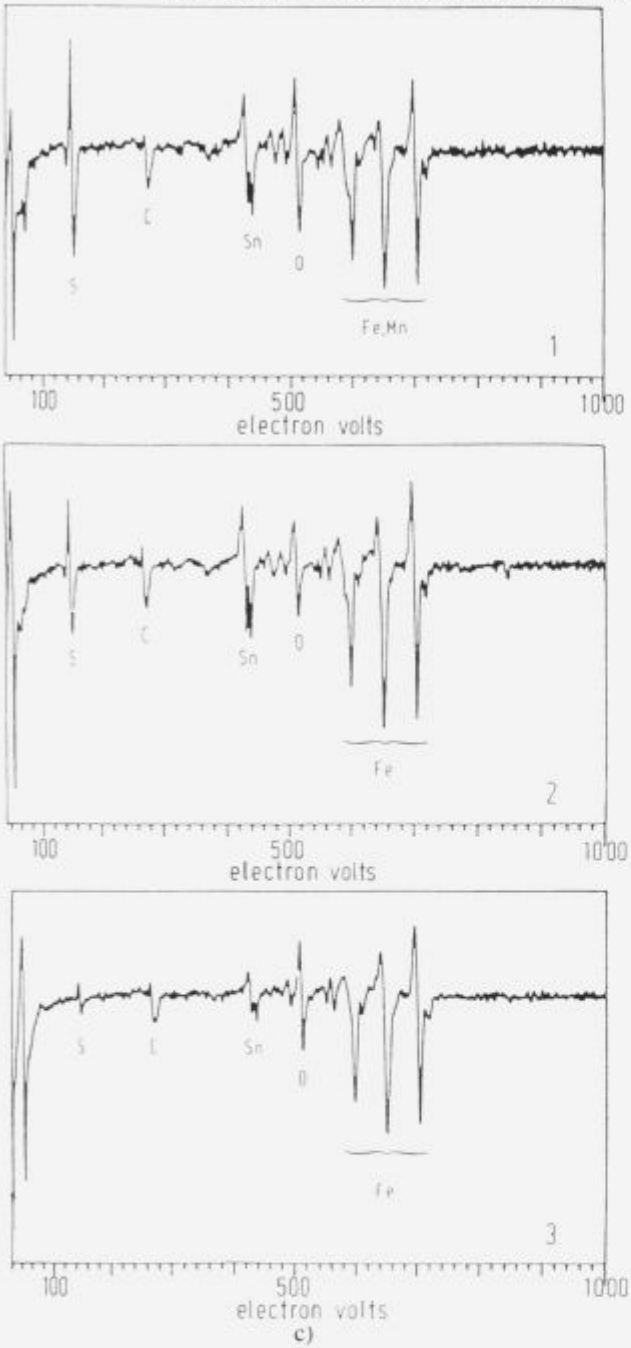

c)

Figure 20. c) AES spectra from the points indicated in a), spectrum 1 MnS particle and cavity surface with Sn, 2 cavity surface with segregated Sn, 3 intergranular fracture face with less Sn

Slika 20. c) AES spektri točk, ki so označene v a), spekter 1 MnS vključek in površina pore z Sn, 2 površina pore s segregiranim Sn, 3 interkristalno prelomljena ploskev z manj Sn

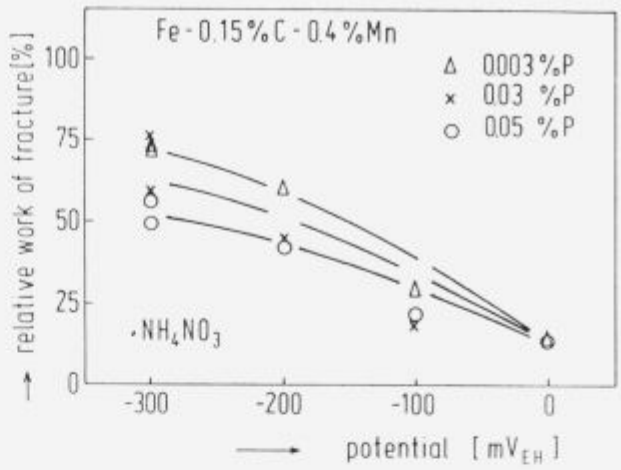

a)

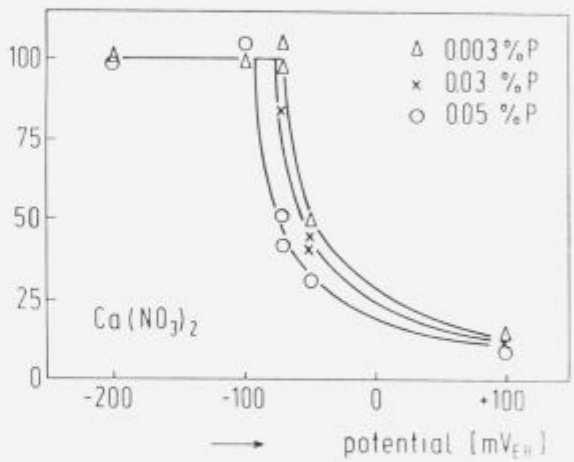

b)

Figure 21. Intergranular stress corrosion cracking of carbon steels, relative work of fracture of carbon steels with different P contents, tested after heat treatment (1 h, 940°C + 48 h, 500°C) in constant-extension-rate tests at 10^{-6}/sec a) in 5N NH_4NO_3, b) in 55% $Ca(NO_3)_2$, both at 75°C

Slika 21. Intergranularna napetostna korozija ogljikovega jekla, relativno delo za prelom ogljikovega jekla z različno vsebnostjo P, določeno po toplotni obdelavi (1 h, 940°C + 48 h, 500°C) pri konstantni stopnji raztezanja 10^{-6}/s a) v 5N NH_4NO_3, b) in 55% $Ca(NO_3)_2$, v obeh primerih pri 75°C

In the production of carbon steels the times usually are short during which the steels are at temperatures in the critical temperature range 400 to 600°C for the grain boundary segregation of phosphorus. The grain boundary concentrations may be somewhat enhanced, for example, after coiling of hot rolled steel at relatively high temperature $\geq$ 500°C.

On the other hand, carbon steels are less susceptible to effects of P than low alloy steels, since carbon in solution displaces phosphorus from grain boundaries. In steels alloyed with carbide forming elements such as Mn and Cr the concentration of dissolved carbon is decreased and thus the grain boundary concentration of phosphorus can be higher (see Chapter 3.1). The effect of Mn on the grain boundary segregation of P was demonstrated, comparing a series of steels with 0.04% Mn and a series of steels with 2% Mn. The phosphorus segregation is enhanced for the high Mn-steels after comparable heat treatment, however, the effect on the IGSCC in nitrates is less pronounced than expected.

In 33% NaOH at 120°C the corrosion potential is established at about -900 mV_H, the IGSCC is observed at higher potentials, -900 to -500 mV_H. The work of fracture

decreases in the range -900 to -700 mV_H to a minimum value of about 25% for all investigated steels, in this range the resistance against IGSCC is virtually independent of the phosphorus content of the steels. Above -700 mV_H to -500 mV_H the work of fracture increases with increasing potential. This increase is clearly faster for the steels with lower phosphorus content. Thus, in the range -700 mV_H to -500 mV_H the susceptibility against IGSCC in NaOH is enhanced by phosphorus[38,39].

In 1 m H_2SO_4 at cathodic polarization the investigated steels show hydrogen induced stress corrosion cracking. The susceptibility towards HSCC is increased with the phosphorus content and reduced for the higher manganese content. The mode of cracking is transgranular. The susceptibility to HSCC is not related to the grain boundary concentration but to the bulk content of phosphorus. HSCC is correlated to the hydrogen uptake of the steels which increases with the phosphorus content and decreases with the manganese content[40,41].

5 References

[1] H.J. Grabke, G. Tauber, H. Viefhaus: Scr. metall. 9 (1975), 1181

[2] H.J. Grabke, W. Paulitschke, G. Tauber, H. Viefhaus: Surf. Sci. 63 (1977), 377

[3] H.J. Grabke, H. Viefhaus, G. Tauber: Arch. Eisenhuttenwes. 49 (1978), 391

[4] H.J. Grabke: Mat. Sci. Engg. 42 (1980), 91

[5] H. Viefhaus, H.J. Grabke: Surf. Sci. 109 (1981), 1

[6] H. de Rugy, H. Viefhaus: Surf. Sci. 173 (1986), 418

[7] M. Rüsenberg, H. Viefhaus: Surf. Sci. 159 (1985), 1

[8] B. Egert, G. Panzner: Surf. Sci. 118 (1982), 345

[9] B. Egert, G. Panzner: Phys. Rev. B 29 (1984), 2091

[10] G. Panzner, B. Egert: Surf. Sci. 144 (1984), 651

[11] B. Egert, H.J. Grabke, Y. Sakisaka, T.N. Rhodin: Surf. Sci. 141 (1984), 397

[12] G. Panzner, W. Diekmann: Surf. Sci. 160 (1985), 253

[13] G. Panzner, D. Mueller, T.N. Rhodin: Phys. Rev. B 32 (1985), 3472

[14] W. Diekmann, G. Panzner, H.J. Grabke: Surf. Sci. 218 (1989), 507

[15] G. Tauber, H.J. Grabke: Ber. Bunsenges. Phys. Chem. 82 (1978), 298

[16] J. Küpper, H. Erhart, H.J. Grabke: Corros. Sci. 21 (1981), 227

[17] H. Erhart, H.J. Grabke: Metal Sci. 15 (1981), 401

[18] H. Erhart, H.J. Grabke: Scr. metall. 15 (1981), 531

[19] H. Erhart, H.J. Grabke, R. Möller: Arch. Eisenhuttenwes. 52 (1981), 451

[20] H. Viefhaus, R. Möller, H. Erhart, H.J. Grabke: Scr. metall. 17 (1983), 165

[21] H.J. Grabke, H. Erhart, R. Möller: Microchimica Acta, Wien, Suppl. 10 (1983), 119

[22] H. Erhart, H.J.Grabke, R. Möller: Arch. Eisenhuttenwes. 54 (1983), 285

[23] R. Möller, H.J. Grabke: Scr. metall. 18 (1984), 527

[24] R. Möller, H. Erhart, H.J. Grabke: Arch. Eisenhuttenwes. 55 (1984), 543

[25] M. Paju, R. Möller: Scr. metall. 18 (1984), 813

[26] W. Jäger, H.J. Grabke, Jin Yu: Proc. Int. Conf. on "Residuals and Trace Elements in iron and Steel", Portorož, Oct. 1985, ed. by F. Vodopivec, Inst. Metall., Ljubljana (1986), 587

[27] R. Möller, S.S. Brenner, H.J. Grabke: Scr. metall. 20 (1986), 587

[28] H.J. Grabke, R. Möller, H. Erhart, S.S. Brenner: Surf. Interface Anal. 10 (1987), 202

[29] H. Hänsel, H.J. Grabke: Scr. metall. 20 (1986), 1641

[30] M. Paju, H. Viefhaus, H.J. Grabke: Steel Res. 59 (1988), 336

[31] M. Paju, H.J. Grabke: Mat. Sci. Techn. 5 (1989), 148

[32] M. Paju, H.J. Grabke: steel research 60 (1989), 41

[33] H.J. Grabke, E.M. Petersen, S.R. Scrinivasan: Surf. Sci. 67 (1977), 501

[34] M. Guttmann: Surf. Sci. 53 (1975), 213 and Mater. Sci. Engg. 42 (1980), 227

[35] R.R. de Avillez, P.R. Rios: Scr. metall. 17 (1983), 677

[36] W.G. Hartweck, H.J. Grabke: Scripta Met. 15 (1981), 653

[37] Jin Yu, H.J. Grabke: Met. Sci. 17 (1983), 389

[38] H.J. Krautschick, H. Bohnenkamp, H.J. Grabke: Werkstoffe u. Korrosion 38 (1987), 103

[39] H.J. Krautschick, H.J. Grabke, W. Diekmann: Corros. Sci. 28 (1988), 251

[40] R.K. Dayal, H.J. Grabke: Steel Res. 58 (1987), No. 4, 179

[41] R.K. Dayal, H.J. Grabke: Werkstoffe u. Korrosion 38 (1987), 409